Journal of Membrane Science 637 (2021) 119524

Contents lists available at ScienceDirect

Journal of Membrane Science

journal homepage: www.elsevier.com/locate/memsci

Comparing amine- and ammonium functionalized silsesquioxanes for large scale synthesis of hybrid polyimide high-temperature gas separation membranes

Farzaneh Radmanesh [a], Monika Pilz [b], Luca Ansaloni [c], Thijs A. Peters [c], Eric Louradour [d], Henk van Veen [e], Dag Høvik [f], Mark A. Hempenius [g], Nieck E. Benes [a,*]

[a] Membrane Science and Technology Cluster, Faculty of Science and Technology, MESA+ Institute for Nanotechnology, University of Twente, P.O. Box 217, 7500, AE Enschede, the Netherlands
[b] Department of Process Technology, SINTEF Industry, Oslo, Norway
[c] Department of Sustainable Energy Technology, SINTEF Industry, Oslo, Norway
[d] CTI, ALSYS Group, Salindres, France
[e] Expertise Group Biomass & Energy Efficiency, Unit TNO-Energy Transition, Petten, the Netherlands
[f] Funzionano AS, Hydrovegen 67, 3936, Porsgrunn, Norway
[g] Sustainable Polymer Chemistry, Faculty of Science and Technology, MESA+Institute for Nanotechnology, University of Twente, P.O. Box 217, 7500, AE Enschede, the Netherlands

ARTICLE INFO

Keywords:
Gas separation
Polyimide
Thermal stability
POSS
Interfacial polymerization

ABSTRACT

PolyPOSS-imide membranes are promising for separating H_2 from larger molecules (CO_2, N_2, CH_4) at temperatures up to 300 °C. Their fabrication involves two steps: interfacial polymerization of POSS and 6FDA, followed by thermal imidization. This work provides a systematic study of the effects of cations on membrane properties and performance. For this, two distinct POSS molecules were used: functionalized with -$NH_3^+Cl^-$ or, so far unexplored, -NH_2. The ammonium groups are partially deprotonated by using three different bases, LiOH, NaOH, and KOH. We demonstrate that the introduced cations affect the film thickness but not the molecular composition of the polyamic acid. All polyamic acids can be imidized, but the cations reduce the imidization kinetics as well as the loss of organic crosslinkers. For flat disc membranes, at 200 °C, the absence of cations results in comparable permeability combined with higher selectivity for H_2/N_2. This, and the possibility to discard adding a base, motivated a scale-up study of the new POSS. For tubular membranes, much higher ideal and mixed gas selectivities are found than for membranes where NaOH was added. Results indicate that the new route allows more reproducible production of defect free membranes and has potential for larger-scale polyPOSSimide fabrication.

1. Introduction

Global warming, due to greenhouse gas emissions, is one of the current worldwide concerns [1]. The development of new, innovative, and flexible methods to reduce emissions of CO_2 in industrial processes at high temperatures is very important. Besides, in many industrial processes, gas separation at elevated temperatures is desirable to reduce efficiency losses associated with cooling and heating of gas streams [2]. Within this context, membrane separations may offer valuable alternatives for existing technologies.

Polyimide membranes are promising candidates for H_2 separation (H_2/N_2, H_2/CH_4, H_2/CO_2) at high temperatures, thanks to their exceptional thermal, chemical, and mechanical stability [3,4]. However, conventional polyimides are not able to properly separate H_2 from mixtures at elevated temperatures. One way to address this issue is by improving the crosslinking density of polyimide, by introducing a highly functionalized and rigid monomer into the macromolecular structure in order to reduce the molecular dynamics [5]. Polyhedral oligomeric silsesquioxane (POSS) with a basic formula of $R_nSi_nO_{1.5n}$ (n = 6, 8, 12), providing eight functionalize groups, offers this possibility [6].

Raaijmakers et al. [7] have used POSS cages as the main building block for synthesizing a polyimide polymeric network, resulting in

* Corresponding author.
E-mail address: n.e.benes@utwente.nl (N.E. Benes).

https://doi.org/10.1016/j.memsci.2021.119524
Received 31 March 2021; Received in revised form 28 May 2021; Accepted 8 June 2021
Available online 2 July 2021

hybrid membranes that can selectively separate gas molecules at elevated temperatures. They have demonstrated a two-step procedure for synthesizing a hybrid polyPOSS−imide network: the interfacial polymerization (IP) of an ammonium chloride salt functionalized POSS and anhydride, followed by thermal imidization. This results in ultrathin (<100 nm) selective films on top of ceramic supports, providing for high H_2 permeance (>1000 GPU) while still retaining gas selectivity of approximately 5 for H_2/CH_4 and H_2/N_2 at 300 °C. The CO_2/CH_4 selectivity of approximately 60 at temperatures below 100 °C emphasizes the applicability of the polyPOSS−imide over a broad temperature range [7].

The procedure of Raaijmakers [7] involves the addition of a base for partial deprotonation of the ammonium groups of the distinguished POSS molecule. The extent of the deprotonation, and the reactivity of the functional groups of the POSS molecules, will be affected by the nature of the cations that are added with the alkaline base. In addition, such cations affect the electrostatics during the interfacial polycondensation reaction, both with respect to the characteristics of the interface between the two immiscible liquids phases with respect to the polymerization kinetics [8–10]. This may affect film properties, such as thickness, free volume, degree of crosslinking, amongst others [11]. Moreover, in the subsequent thermal treatment of the polyamic acid films, the presence and nature of the cations can also impact the properties of the final materials. The condensation of the amic acid bonds to form the imide groups cannot occur when the proton of the amic acid group is exchanged with another cation; the imidization requires a carboxylic acid group in ortho position to an amide group which is blocked by the ions [12–14]. Also, the cation interferes with intra and intermolecular interactions of polyamic acid groups, for instance, diminishing hydrogen bonding. This also affects the subsequent imidization of the polyamic acid [15]. Finally, ions that remain in the final membrane could facilitate the sorption of small polar molecules such as water, affecting the transport of these and other small molecules within the matrix (e.g., competitive sorption, hindrance of diffusive pathways).

By using a proprietary approach, SINTEF is able to synthesize POSS molecules with amine groups (POSS–$(CH_2)_3NH_2$), rather than POSS with ammonium groups POSS (POSS–$(CH_2)_3NH_3^+Cl^-$) that require deprotonation [16]. This allows omitting the addition of a base in the procedure reported by Raaijmakers [7]. Here, we investigate whether such a more facile method, with the new POSS source, can be used for membrane fabrication. For this purpose, the two different types of POSS are reacted with 4,4-(hexafluoroisopropylidene) diphthalic anhydride (6FDA), atop ceramic supports. Deprotonation of the ammonium functionalized POSS is done with the addition of different bases, *i.e.*, LiOH, NaOH, and KOH, individually, introducing different cations. This allows studying the effect of the nature of the cations on the formation, imidization, and performance of polyPOSS-imide membranes for H_2 recovery. Finally, the scale-up potential of membranes deploying the new POSS source is investigated using porous ceramic tubular supports. The performance of these tubular membranes is assessed by means of single and mixed gas measurements in a wide range of operating conditions.

2. Experimental

2.1. Materials

Toluene (anhydrous 99.8 wt%), 6FDA, NaOH, LiOH, and KOH were obtained from Sigma-Aldrich. Ammonium chloride salt functionalized POSS (Octa ammonium POSS®, USA) was purchased from Hybrid Plastics, abbreviated HP-POSS. Octa aminopropyl POSS (52.6 wt% in n-propanol) was kindly provided by SINTEF (Norway), abbreviated SF-POSS, and recently up-scaled by Funzionano AS (Norway). Porous α-alumina discs (D 39 mm, thickness 2 mm) were obtained from Pervatech B.V. (The Netherlands), coated with a 3 μm thick γ-alumina layer via a dip-coating and calcination process as described before by Karaliç et al. [17] and used as supports. Asymmetric TiO_2/Al_2O_3 single-channel (OD = 10 mm, ID = 6 mm, length = 250 mm) supports were provided by Céramiques Techniques Industrielles (CTI, France) and coated with a γ-alumina layer atop of an internal zirconia microfiltration layer.

2.2. Material fabrication

For both the preparation of freestanding films and membranes, the pH value of aqueous solution of HP-POSS (0.9 wt%) was adjusted to 9.9 by using one of the base solutions, NaOH, LiOH, and KOH, with a concentration of 0.5 M. For SF-POSS, the 0.9 wt% aqueous solution has an initial pH of 10.5, and no additional pH adjustment was needed. Thin films were prepared by 2 step procedures reported elsewhere [18,19]: first, the interfacial polymerization reaction between 0.9 wt% POSS in water and 0.075 wt % 6FDA in toluene, resulting in the formation of polyamic acid, followed by a thermal imidization. Based on the type of POSS solution, different abbreviations were used, which can be found in Table 1.

2.2.1. Preparing freestanding films

The freestanding films were prepared by bringing the pH adjusted aqueous solution of HP-POSS into contact with the 6FDA solution of 0.075 wt% in toluene. After 30 min, the collected film was washed with acetone and water. It was followed by imidization at 300 °C for 2 h with a ramp rate of 5 °C/min in air atmosphere. The collected solid might be referred to as powder in the text.

2.2.2. Membranes preparation

In brief, a film was formed atop a flat disc ceramic membrane by soaking the porous support in 0.9 wt% POSS aqueous solution for 15 min, followed by contacting it with the 6FDA solution in toluene. Subsequently, the membrane was imidized by heating it to 300 °C for 2 h with a ramp rate of 5 °C/min in an air atmosphere.

For the tubular membranes, the same procedure as in Ref. [19] was used. The tubular membranes were pre-wetted with 0.9 wt% aqueous SF-POSS solutions for 15 min, followed by reacting the 6FDA solution for 5 min. Subsequently, imidization of the membranes was carried in an oven for 2 h at 300 °C.

2.3. Material characterization

Scanning electron micrographs were obtained using a field emission scanning electron microscope (FE-SEM, JSM-7610F, Jeol) to visualize the samples' morphology and thickness. The images were taken after applying a 5 nm Pt/Pd coating.

Thermal gravimetric analysis (TGA) combined with mass spectrometer (MS) measurements were carried out using a Netsch STA 449 F3 Jupiter TGA and QMS 403 D Aelos MS under 70 mL min^{-1} N_2 flow with a heating rate of 10 °C min^{-1} from 50 to 800 °C.

Fourier transform infrared spectroscopy (FTIR) in attenuated total reflectance (ATR) was performed to analyze the structure of the membranes in the range of 400–4000 cm^{-1} using (ATR-FTIR, Spectrum Two,

Table 1
List of acronyms.

Acronym	Name
M^+	Metal cation, Li^+, Na^+, K^+
PA	Polyamic acid prepared with SF-POSS
Li-PA	Polyamic acid prepared with HP-POSS, pH adjusted with LiOH
Na-PA	Polyamic acid prepared with HP-POSS, pH adjusted with NaOH
K-PA	Polyamic acid prepared with HP-POSS, pH adjusted with KOH
M-PA	Polyamic acid prepared with HP-POSS, pH adjusted with different bases (M-pH)
PI	Polyimide prepared from PA
Li-PI	Polyimide prepared from Li-PA
Na-PI	Polyimide prepared from Na-PA
K-PI	Polyimide prepared from K-PA
M-PI	Polyimide prepared from M-PA

PerkinElmer).

X-ray Photoelectron Spectroscopy (XPS) measurements were performed on the membranes with an Ultra Axis™ spectrometer (Kratos Analytical, Manchester UK). The membranes were irradiated with monochromatic Al K_α radiation (1486.6 eV) with a beam size of 100 μm at a power of 25 W.

X-ray diffractometer (XRD) patterns were recorded by monitoring the diffraction angle 2θ from 5° to 40° on a D2 PHASER XRD (Bruker) using copper radiation under a voltage of 45 kV and a current of 40 mA.

EDX analysis was carried out at 10 kV with >1000 counts s^{-1} on obtained powders (SEM, JSM-6010LA, JEOL). The experiment was repeated four times for each sample. The average value and 95% confidence interval are reported.

2.4. Membrane performance

2.4.1. Flat disc membranes

Membrane single gas permeation experiments were done using Inspector Poseidon (Convergence, The Netherlands) gas permeation setup using a dead-end mode at a *trans*-membrane pressure of 2 bar and atmospheric pressure at the permeate side. Single gas permeation of He, N_2, H_2, CH_4, and CO_2 was measured at temperatures between 50 and 200 °C. Two different samples were measured, and the average data and standard deviation are reported. The ideal selectivity was calculated as the ratio of respective permeances.

2.4.2. Tubular membranes

Single-channel membranes were tested in a home-build gas permeation setup available at SINTEF, in a crossflow configuration, reported elsewhere [19]. In short, the feed gas was applied on the inner side of the membranes (lumen) with an active permeation area of 23 cm^2. Mass flow controllers (MFC, Bronkhorst High-Tech B·V., The Netherlands) and a back-pressure regulator (BPR, Bronkhorst High-Tech B·V., The Netherlands) were used to accurately control the gas feed flow and control its pressure, respectively. The permeate stream was kept at ambient pressure. The gas flow rates were measured with mass flowmeters (MFM, Bronkhorst High-Tech B·V., The Netherlands). Single gas permeation of N_2, H_2, CH_4, and CO_2 was measured up to 250 °C and 10 bar. For the mixed gas measurement, a gaseous mixture containing 60% H_2, 20% CH_4, 10% N_2, and 10% CO_2 was used to mimic the conditions of coke oven gas. The gas concentration in all the gaseous streams (feed, retentate, and permeate) was measured by a micro-GC (μGC, Agilent 490). The reported data is the average result of three tubular samples and denoted GEN-PI.

The gas permeance of the *i*-th gas, P_i, was obtained using Equation (1):

$$P_i = \frac{\dot{n}_p \; y_{p,i}}{A \Delta p_i} \tag{1}$$

where $\dot{n}_p$ is the total mass flow of the permeate side, $y_{p,i}$ is the *i*-th gas concentration on the permeate side, A is the membrane area, and Δp_i is the differential *i*-th gas partial pressure between the feed and the permeate side. For gaseous mixture, the Δp_i is calculated from Equation (2):

$$\Delta p_i = \frac{\left(p_{f,in} - p_p\right)_i - \left(p_{f,out} - p_p\right)_i}{\ln\left(p_{f,in} - p_p\right)_i - \ln\left(p_{f,out} - p_p\right)_i} \tag{2}$$

where $p_{f,in}$ and $p_{f,out}$ are the pressure at the feed inlet and outlet, respectively.

For the gas mixture, the selectivity was obtained by means of Equation (3):

$$\text{Selectivity of i over j} = \frac{y_i / y_j}{x_i / x_j} \tag{3}$$

where *y* and *x* are the gas concentration of the species i in the permeate (*y*) and in the feed (*x*) stream, respectively.

The stage cut for the separation experiment was calculated as the ratio between the gas flow on the permeate side and the feed side, as shown in Equation (4):

$$\text{stage cut} = \frac{\dot{n}_p y_{p,i}}{\dot{n}_f y_{f,i}} \tag{4}$$

3. Results and discussion

In this work, the results and discussion part is divided into three parts. Firstly, we study the effect of cations on the formation and properties of polyamic acid and polyimide networks and the imidization step. Secondly, the gas permeation performance of small flat disc membranes is characterized. Finally, in the third part, the gas separation performance of tubular membranes is evaluated.

3.1. Characterization of the polymeric network

Fig. 1 gives a schematic representation of the preparation of freestanding polyPOSS-imide films. Reactions were so rapid that the formation of the freestanding polyamic acid films between the two immiscible solutions could be easily confirmed with the bare eye in less than 1 min. The formed polyamic acid layer was converted to polyimide by the dehydrative cyclization of the polyamide acid through thermal imidization.

Fig. 2A represents the FTIR spectra of polyamic acid and polyimide powders normalized with respect to the symmetric stretching of CF_3 band at 1256 cm^{-1}. The bands at 1624 cm^{-1} and 1555 cm^{-1} exhibit N-H bending and C=O stretching of the amic acid group in all samples, respectively. A single peak at 1118 cm^{-1} for νSi–O–Si is expected for perfect symmetry of the Si–O skeleton, but split into two split peaks [16], mainly due to the loss of that perfect skeleton symmetry upon reaction-induced variations of the chemical environment at a certain degree of crosslinking. Two bands at 1099 cm^{-1} and 1032 cm^{-1} are attributed to the Si-O-Si asymmetric stretching of polyhedral silsesquioxane structures, respectively. For all the samples, except for PA, a peak appears around 1410 cm^{-1} that can be attributed to the C-O stretching of carboxylic acid groups in which the proton has been exchanged for a cation [12,20,21]. Fig. S1 represents a schematic illustration of the cation exchange process of polyamic acids.

Fig. 2B shows the FTIR of polyimide powder, normalized for the CF_3 band. After heating the polyamic acids to 300 °C for 2 h, two new peaks appear at 1778 cm^{-1} and 1710 cm^{-1} attributed to C=O symmetric and asymmetric stretching of the imide group. Thus, FTIR indicates the successful formation of all polyamic acid and polyimide networks. Also, for the polyamic acid networks fabricated with HP-POSS, it confirms the presence of carboxylate salts due to proton-cation exchange of the carboxylate acid groups.

EDX analysis is used on the formed networks to investigate the elemental composition and extent of crosslinking for polyamic acid and polyimide powders (Table 2). The data reveal the presence of Na, K, C, Si, Cl, O, and F. Unfortunately, Li cannot be detected with this method due to the low x-ray yield of this element [22]. Elemental analysis reveals that the PA does not contain significant amounts of cations or chloride. For the M-PA powders in which a base was added during synthesis, the corresponding cations are detected, as well as Cl^-. The detected cations, M^+, can be presented in the form of M^+-carboxylate groups or as the remaining MCl that was formed during the IP reaction. This is confirmed by XRD data, Fig. S2, where distinct peaks corresponding to the salts' crystal structure indicate that MCl salt is present in an amorphous M − PI network. The similar elemental content of M^+ and Cl^- do not necessarily imply that the cations are predominantly present as MCl; the chlorine can also be present accompanied by a proton. Also,

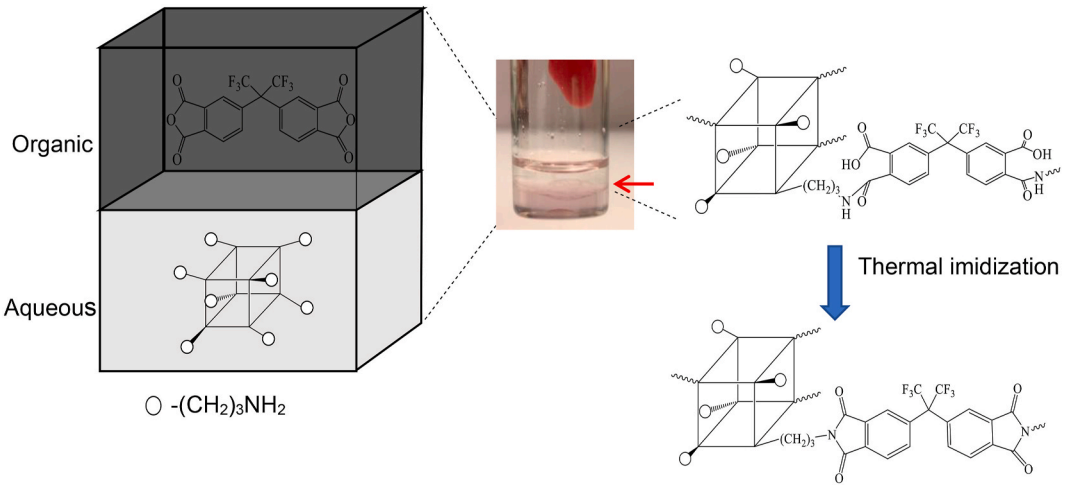

Fig. 1. Schematic representation of the preparation of freestanding polyPOSS imide films; for supported membrane films a porous support structure is soaked with the aqueous solution and subsequently contacted with the organic solution, the POSS cage is illustrated as a cube.

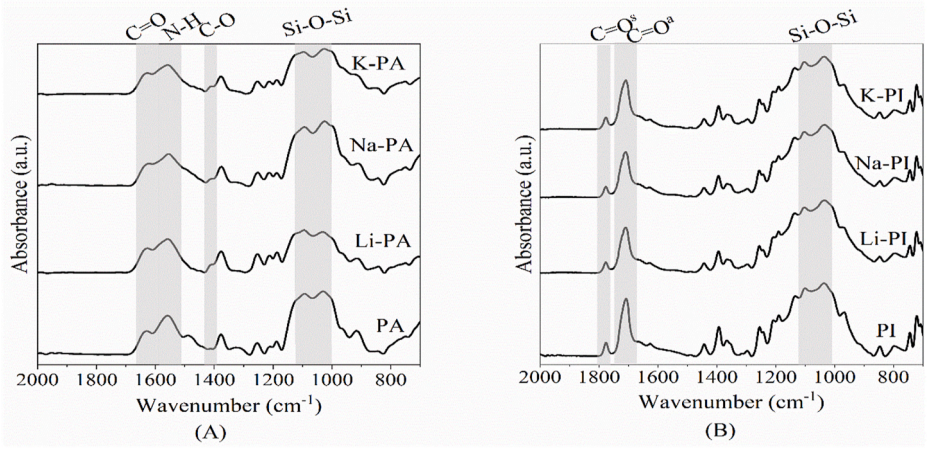

Fig. 2. FTIR spectra of (A) polyamic acid and (B) polyimide powders. In the spectra of the polyamic acid (A), the peak at 1410 cm^{-1} indicates dissociated carboxyl groups in the M-PA film. For polyimide spectra (B), the new peaks at 1778 cm^{-1} and 1710 cm^{-1} correspond to the imide groups.

Table 2
EDX analysis of polyamic acid and polyimide powders.

Elemental Composition (%)								
Polyamic acid					Polyimide			
	PA	Li-PA	Na-PA	K-PA	PI	Li-PI	Na-PI	K-P
Na	0	0	1 ± 0.2	0	0	0	0.72 ± 0.3	0
K	0	0	0	0.5 ± 0.2	0	0	0	0.1
Cl	0	0.3 ± 0.1	1.3 ± 0.3	0.9 ± 0.2	0	1.2 ± 0.3	0.7 ± 0.2	0.1
C	54.6 ± 2.4	53.2 ± 1.7	55.9 ± 2.1	52.8 ± 2.1	46.1 ± 2.4	57.5 ± 5.1	54.1 ± 0.5	53.8 ± 0.1
N	11.5 ± 1.4	12.3 ± 3.1	9 ± 2	11.9 ± 1.7	9.2 ± 1.2	6 ± 1.6	7.6 ± 0.6	8.1 ± 0.7
Si	7.3 ± 2.1	5 ± 1.8	7.8 ± 2.4	6.4 ± 1.2	10.2 ± 2.7	9.5 ± 3.1	8.3 ± 0.9	7.4 ± 2.5
F	7.7 ± 1	9.3 ± 0.9	7.9 ± 0.5	7.7 ± 1	5.1 ± 0.4	8 ± 1.5	9.4 ± 0.8	9.5 ± 2.1
F/Si	1.2 ± 0.3	1.8 ± 0.6	1 ± 0.3	1.2 ± 0.1	0.5 ± 0.2	0.9 ± 0.3	1.1 ± 0.1	1.3 ± 0.5
O	18.8 ± 2.3	19.9 ± 0.4	17.1 ± 1.5	19.8 ± 2.3	29.3 ± 4.6	18.9 ± 2.3	19.2 ± 1.9	21.2 ± 1.3

the content of Na is higher than K, attributed to the higher affinity of carboxylic acid toward Na [23].

The F/Si ratio is similar for all the polyamic acids. This ratio is representative for the degree of crosslinking, and the result implies that, in the interfacial polycondensation process, a similar amount of functional groups on the POSS cage will react with an anhydride group, irrespective of the presence and type of the cation and the presence of Cl^-. In other words, the presence of the cations does not substantially affect the molecular composition of the polymer that is formed in the interfacial polymerization reaction.

Also, in the derived polyimide material, the main elements of interest (Na, K, C, Si, Cl, O, and F) are detected. For all polyimides in which cations were added (M – PI), the changes in the concentrations of C, F, Si and O remain within experimental error, indicating no significant loss of crosslinker groups. The ratio of F over Si stays constant over the imidization process (around 1.1). This indicates that the POSS cages are, on

average, connected with 3–4 bridges, but the experimental error is large. These results are in line with a previous study [18]. Notably, for PI samples, the percentage of C and F are slightly lower, and the content of Si and O are slightly higher than in the corresponding polyamic acid (PA). The thermal treatment reduces the ratio of F/Si to 0.5, corresponding to less than 3 imide groups per POSS cage, but again the experimental error is large. Still, these results indicate that thermal imidization can result in the loss of more of the organic crosslinkers in the absence of the cations.

XPS is performed on the surface of four membranes, PA, PI, Na-PA, and Na-PI, and the results are listed in Table 3. The data reveal the presence of POSS and anhydride for all samples. As expected, for PA and PI no Na is detected, and Na-PA and Na-PI do contain Na. After imidization, XPS results reveal, for both samples, decreased content of C and F and increased content of Si and O. The F/Si ratios are reduced by an order of magnitude for both samples. This implies that during thermal imidization, at the outer surface of the membranes, the extent of crosslinking is significantly decreased. Such a decrease in crosslinks is in contrast with the EDX results, where only small changes in crosslinker concentration are observed, even in the absence of the cations. It should be emphasized that XPS probes only a very thin (~nm) region at the outer surface of the supported membranes, whereas EDX probes the bulk composition of the freestanding films. It has previously been observed that the degree of crosslinking in the thin outer surface region of polyPOSSimide membranes is lower as compared to in the rest of the films [24].

The TGA data in Fig. 3A shows the mass loss of 4 different polyamic acids. All polyamic acids exhibit four steps of mass loss up to 800 °C, agreeing well with previous observations [25]. The mass loss between 150 and 300 °C is higher for the PA sample (10%) as compared to other samples (5%). This is due to more pronounced imidization in the absence of amide groups in which the protons have been exchanged for cations. In polyamic acid containing cations, the replacement of a proton of a carboxylic acid by an M^+ cation prevents from ring closure (imidization). Also, the lower mass loss of the M-PA samples can be due to lesser detachment of linker groups. This can be the result of the stabilization of the CO-NH group by a cation [12] or the reduced hydrogen bonding between the NH and OH of adjacent amide groups induced by the presence of the cations. This hydrogen bonding can lead to destabilization, and hence to an amic acid structure that is more sensitive to thermal imidization [12,15,26].

The thermal stability of the polyimide network is represented by TGA data in Fig. 3B. It can be concluded that all polyimide polymers are thermally stable up to 300 °C, the onset of decomposition, and at a higher temperature, a significant decrease in mass is observed. As expected, PI has a higher amount of residue at 800 °C than the other polyimides. The results are in line with the EDX results and the TGA results for the polyamic acid. They indicate that the PI powders can have fewer organic bridges, leading to a higher final (inorganic) residue at 800 °C. The difference between the mass loss of M − PI and PI, around 7%, is in good agreement with the ratio of 6FDA and POSS derived from the EDX data; based on this ratio, and assuming the loss of all propyl chains and fluorine groups, the difference between the residuals of polyimide powders can be calculated to be 7%. Table 4 shows the T_d^5, T_d^{10}, and T_d^{max} (subscript indicates wt% loss) of the powders. All polyimide samples decompose around 516–538 °C. PI has the highest T_d^5, T_d^{10} because of the lower number of organic bridges between the POSS cages. This leads to about 10–22 °C differences between PI and M-PI.

In summary, all the polyimide networks are stable up to 300 °C, and the difference between the residues and $T_{d,max}$ at 800 °C, originates from the lower amount of organic bridges between the POSS cages in PI polymers.

Table 3
XPS analysis of polyamic acid and polyimide powders.

Elemental Composition (%)				
	Polyamic acid		Polyimide	
	PA	Na-PA	PI	Na-PI
Na	0	1 ± 0.1	0	0.6 ± 0.1
Cl	0	0.7 ± 0.2	0	0
C	65 ± 2.7	59.2 ± 1.7	32 ± 3.1	22 ± 3.7
N	5.7 ± 0.5	5.7 ± 0.3	3.3 ± 0.5	2.1 ± 0.3
Si	5.9 ± 0.5	7.1 ± 1.6	9.3 ± 1.4	6.3 ± 0.7
F	3.5 ± 0.2	6.4 ± 0.4	0.8 ± 0	0.9 ± 0.1
F/Si	0.6 ± 0.1	1.2 ± 0.2	0.08 ± 0	0.14 ± 0
O	19.3 ± 1.1	21.1 ± 1.1	45.5 ± 1.4	54 ± 0.8

3.2. Flat disc membrane characterization and performance

Fig. 4 shows the FE-SEM cross-sectional images of membranes. It confirms the fabrication of the layer atop the ceramic supports. The layer thicknesses are in the range of other IP membranes [27]: Na-PI (69.4 ± 10 nm) ≤ Li-PI (83.9 ± 5 nm) < PI (100.3 ±3 nm) < K-PI (137.8 ± 10 nm).

Different ions induce different electrostatic charge distribution on the interface of the solvents, which is the reaction zone. They make different 'salting-out' and 'salting-in' effects, often following the Hofmeister series. For instance, in this series, K^+ with higher salting-out efficiency would result in a faster layer formation [28]. In addition, the presence and nature of the salt affect the nature of the interface; a less sharp interface between two liquids will affect film thickness [9]. Because of the large experimental error (±10 nm) and a large number of convoluted effects, here we do not analyze in detail the relation between the salt and the film thickness. Yet, the observations are essential to interpret the results in the next section.

Fig. 5 shows the gas permeability behavior of the polyPOSS-imide membranes at 200, 100, and 50 °C. All membranes display molecular sieving behavior; a decreasing permeability with increasing size of the permeant [29]. The persistence of this sieving behavior at elevated temperature is attributed to moderation of the dynamics of the crosslinked network, resulting from the incorporation of the rigid inorganic cages. This is in line with earlier experimental studies [18]. The order of gas permeance is Li-PI, Na-PI > PI > K-PI (Fig. S3), which is in agreement with thicknesses observed in the SEM micrographs. Because of the different membrane thicknesses found for the different M − PI, Fig. S2 provides the thickness-corrected permeability values. The data in this figure reveals similar permeabilities for the different membranes, with slightly lower values for K-PI and PI as compared to Na-PI and Li-PI.

Molecular sieving typically involves a thermally activated diffusion mechanism. The corresponding activation energies obtained from fitting the Arrhenius equation to the data are listed in Table 5. The values vary in the range of 8–25 kJ/mol, which is in good agreement with reported data for polyimide membranes [30]. For all membranes, the trend for activation energies is $CH_4 > N_2 > H_2 > He \geq CO_2$. Generally, gases with higher kinetic diameters have higher activation energies for diffusion. The lowest value for the energy of activation for CO_2, is due to the affinity of these gases with the CF_3 and amine groups. The relatively large sorption energy of this gas reduces the energy of activation [31]. For the other gases, the negative contribution of the enthalpy of sorption is lower.

The PI membrane shows a slightly higher activation energy for N_2 and CH_4 than other membranes. This can be related to a lower number of organic bridges in the PI network, as was found in the EDX and TGA analysis. The only pathway for the diffusion of gases in the networks is via the organic bridges because the POSS cages are too small, even for H_2 molecules [32,33]. The removal and chemical conversion of polyamic acid results in shrinkage and some cases, remove some additional free volume [25]. Fewer organic bridges will thus lower diffusion, particularly for larger molecules. It should be mentioned that the lower concentration of CF_3 and corresponding higher concentration of amines may cancel out, to a certain degree, in the sorption energy of CO_2. As a

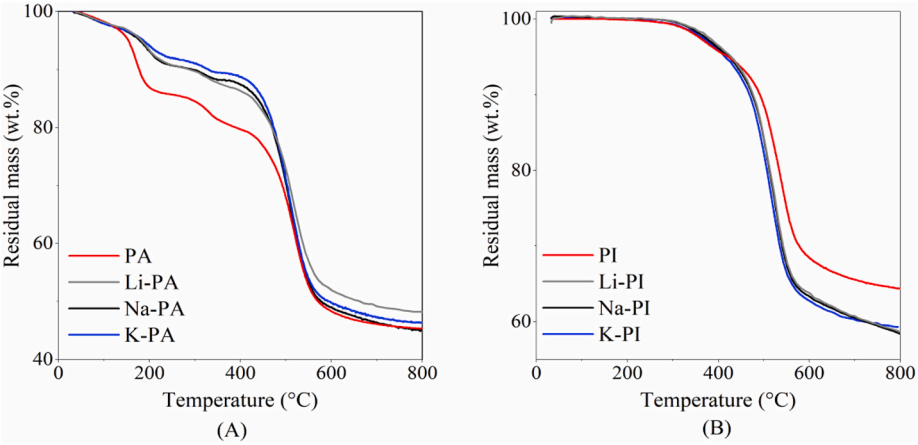

Fig. 3. TGA scan of (A) polyamic acid and (B) polyimide powders.

Table 4
T_d^5, T_d^{10}, $T_{d,max}$, and residue at 750 °C of polyimide.

	K-PI	Na-PI	Li-PI	PI
T_d^5	414	423	424.3	422
T_d^{10}	472	471	473.1	494
$T_{d,max}$	516.3	527.1	520.5	538

result, all the membranes show a comparable value for CO_2 activation energy [34].

Fig. 6 depicts the (single gas) permselectivity of H_2/N_2, H_2/CH_4, and H_2/CO_2 as a function of temperature. The selectivity of all gas pairs decreases as a function of temperature except for H_2/CO_2. This is related to similar activation energies of the H_2 and CO_2 [30]. The selectivity of H_2/CO_2 for all the membranes is comparable; it is not affected by changing the cation during interfacial polymerization.

For the other gases, the energy of activation is large compared to that of H_2. Sieving selectivity persists up to the highest measured temperature (200 °C). This is attributed to the alternating network of organic bridges and rigid POSS cages. At 200 °C, the highest selectivity for H_2/N_2 is observed for the PI (32.9), as compared to Li-PI and Na-PI (both 21) and K-PI (24). For H_2/CH_4 at 200 °C K-PI has the highest selectivity (37.1), followed by PI (25.1) and subsequently Li-PI (18.1) and Na-PI (17.2). Obtained selectivities are comparable to those of polyimide,

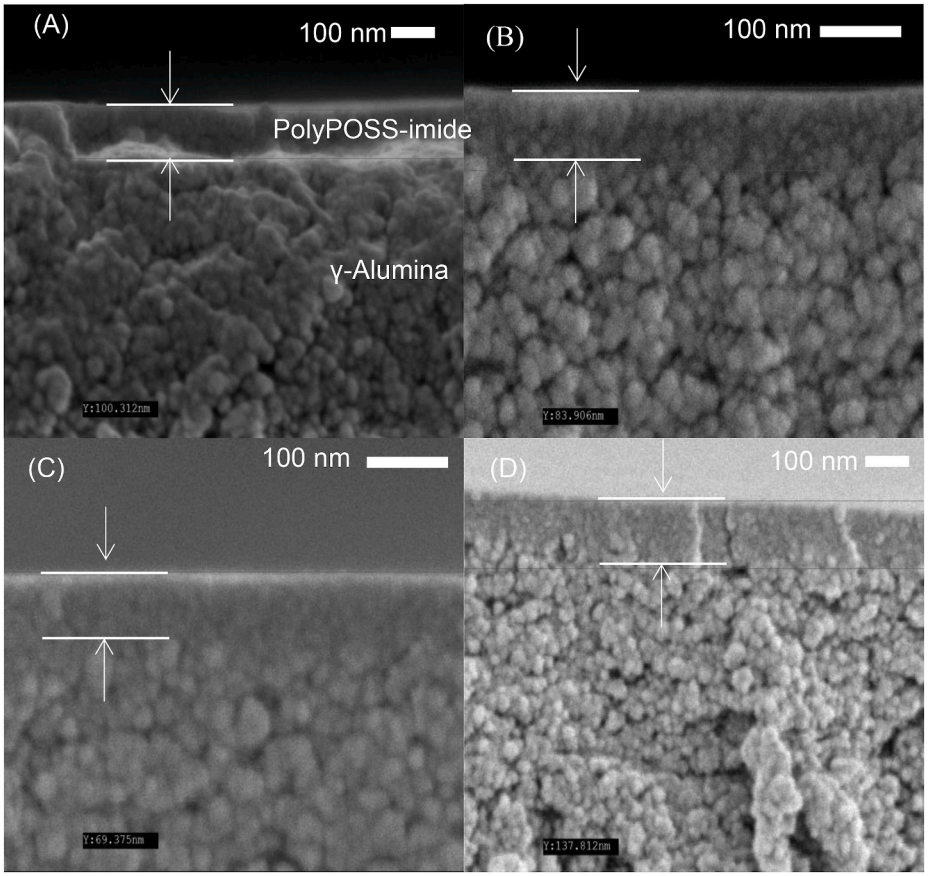

Fig. 4. FE- SEM images of cross-section (a) Li-PI, (b) PI, (c) Na-PI, and (d) K-PI membranes.

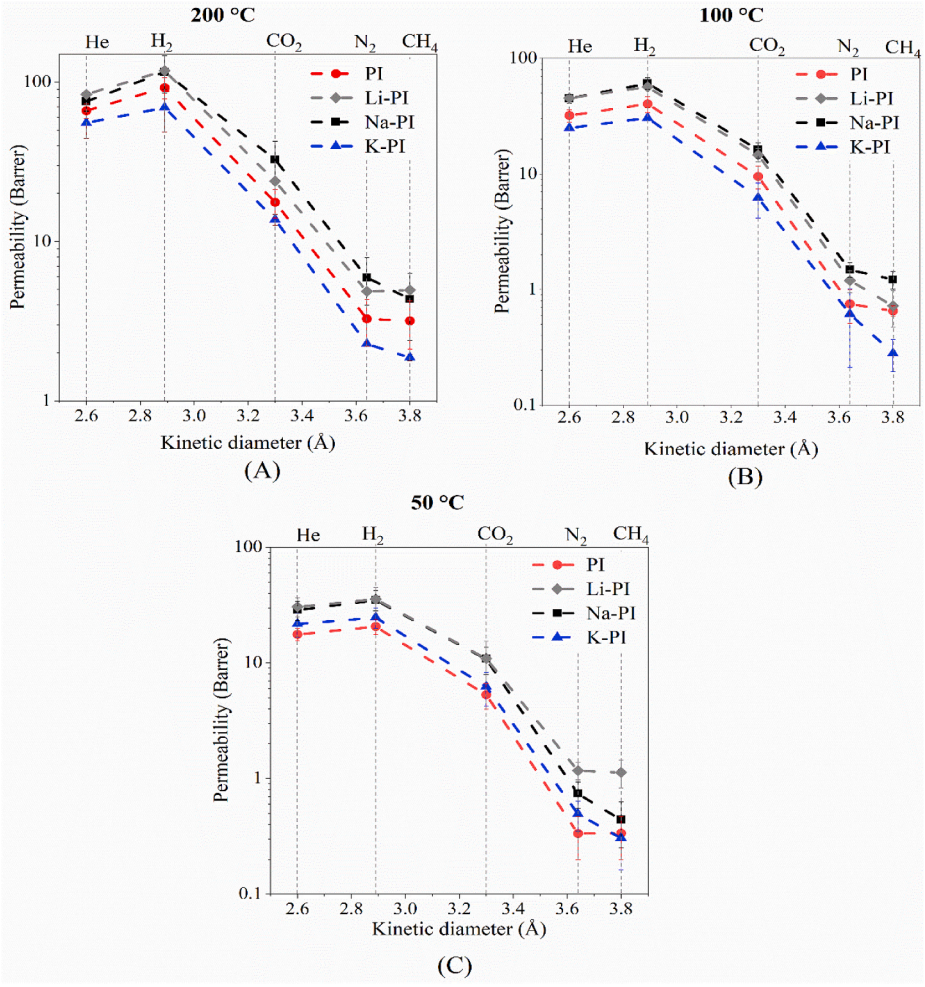

Fig. 5. Gas permeability as a function of the gas kinetic diameter for polyimide membranes at (A) 200 °C, (B) 100 °C, and (C) 50 °C.

Table 5
Calculated activation energies for pure gas permeance based on Arrhenius equation.

Gases	Activation energy (kJ mol^{-1})			
	PI	Li-PI	Na-PI	K-PI
He	11.2 ± 0.2	9.2 ± 0.7	8.7 ± 0.8	11.7 ± 2.1
H_2	12.4 ± 0.4	10.5 ± 0.9	10.4 ± 0.7	12.8 ± 1.1
CO_2	10 ± 0.1	8.7 ± 1.1	8.9 ± 0.8	8.4 ± 1.1
N_2	19.6 ± 0.7	16.9 ± 1.5	18 ± 0.2	16.2 ± 0.6
CH_4	21.5 ± 0.2	18.9 ± 1.5	19.8 ± 0.5	18.2 ± 0.3

Tröger's Base (TB)-based polyimide and poly(*p*-phenylenebenzobisimidazole) [29,35,36]. The high selectivities for PI at high temperature result from the high activation energies, which in turn are attributed to the lower concentration of organic bridges and corresponding free volume available for diffusion.

In summary, all polyPOSS-imide membranes are thermally stable. They have comparable permeabilities with subtle differences in selectivities. Therefore, both SF-POSS and HP-POSS can be used for synthesizing polyPOSS-imide membranes on a large industrial scale. SF-POSS is an interesting monomer to use on an industrial scale to prepare polyPOSS-imide membranes since it provides a more straightforward procedure by omitting the pH adjusting step needed for HP-POSS. In view of this, we will assess the scale-up potential of polyPOSS-imide membranes by using SF-POSS as a monomer.

3.3. Tubular membrane characterization and performance

Fig. 7 shows the cross-sectional SEM images of the inner side of the tubular membrane. The average thickness of polyPOSS-imide layer is 120 nm with thickness variation over the length of ±30 nm, which is notable. This agrees well with the thickness obtained in the previous section for small flat disc membranes. The significant variation in the thickness of tubular membranes is related to the larger size of the support. Comparing GEN-PI and Na-PI from the literature [19] indicates that both membranes have a similar thickness in the range of 90–150 nm, unlike the flat disc membranes with a noticeable standard deviation. While producing a more homogeneous layer is more manageable for small flat disc supports (area of 11.9 cm^2), more effort is needed to better control the fabrication on tubular supports (area of 43 cm^2) or even multichannel supports [19]. It should be mentioned that more data is needed for a complete comparison between the layer's thickness atop flat and tubular supports.

Fig. S4A shows single gas performance data of GEN-PI as a function of temperature at a transmembrane pressure of 10 bar. It can be observed that the performance of the tubular membrane agrees well with the performance of the flat disc membranes in the previous section. This is in line with earlier experimental studies [19]. The permeance decreases with increasing the kinetic diameter of the permeating gas. Also, at higher temperatures, the permeance increases, which shows the dominant diffusion mechanism of gas transport in the membranes. Both flat disc and tubular membranes reveal remarkably similar results in terms of permeances. The activation energies are represented in Table 6,

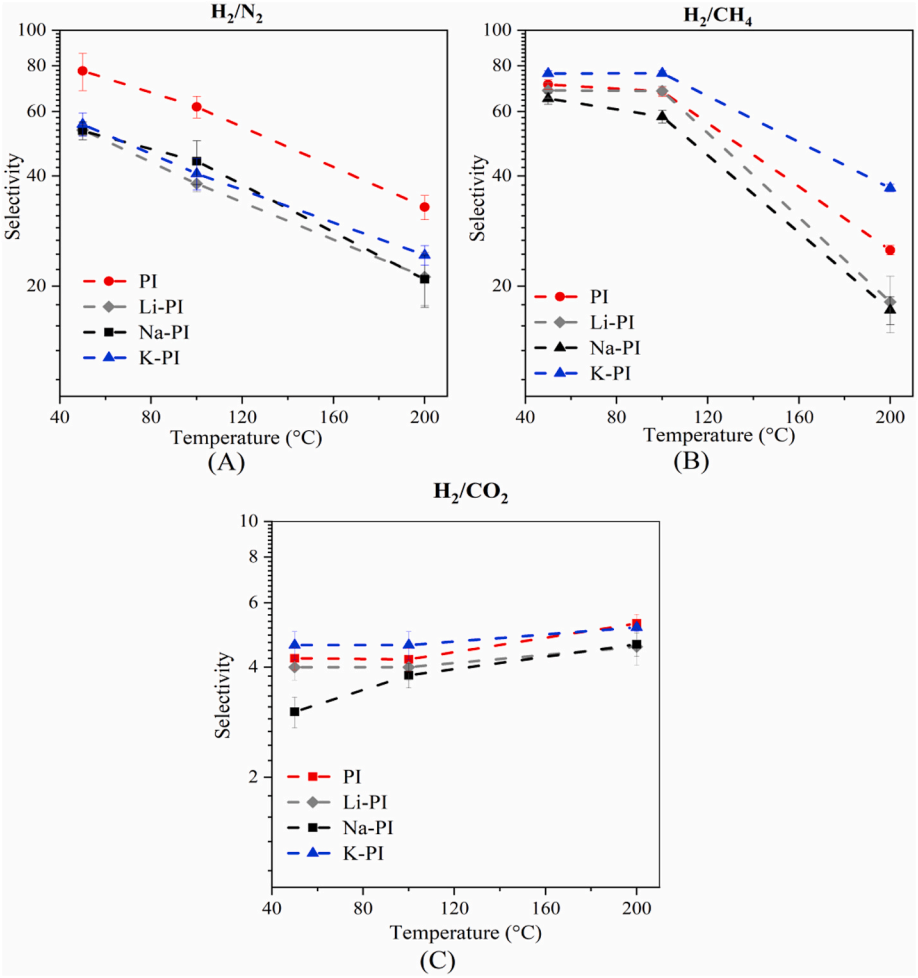

Fig. 6. Ideal selectivity of (A) H_2/N_2, (B) H_2/CH_4, and (C) H_2/CO_2 as a function of temperature.

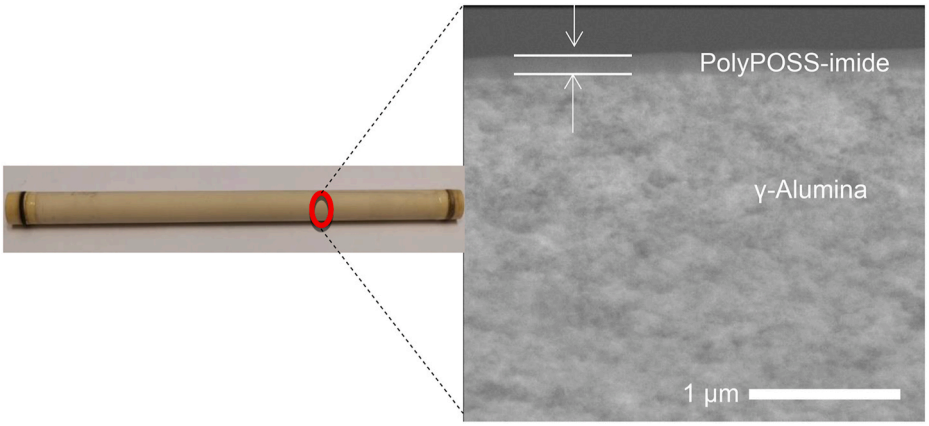

Fig. 7. SEM images of the cross-section of a tubular polyPOSS imide-membrane, GEN-PI.

and it follows the same trend as the flat disc membranes, $CH_4 > N_2 > H_2 \geq CO_2$. For all gases, the obtained activation energies are moderately higher compared to the flat disc membranes. It could be related to reduced mass transport resistance of the tubular membranes compared to their disc-shaped counterparts and higher operating pressure (10 bar) [19]. Comparing the results with Na-PI tubular membranes in literature [19] reveals that the activation energies for GEN-PI are considerably higher, agreeing with flat disc membranes in section 3.2. As explained in the previous section, the structural changes in PI compared to Na-PI

Table 6
Pure gas activation energies calculated based on Arrhenius equation.

Gases	Activation energy (kJ mol^{-1})
H_2	19.9 ± 0.9
CO_2	22.1 ± 1.5
N_2	30.4 ± 1
CH_4	32.9 ± 0.9

result in higher activation energies and underline the higher energy barrier for gas diffusion.

Fig. 8 shows the influence of temperature and pressure on the performance of the tubular GEN-PI membrane, and compares it with the literature data of Na-PI [19]. As mentioned before, this section aims to evaluate the performance of thin films for upscaling, and all the performance data is reported based on the membrane permeance. For all temperatures, the same H_2 permeance trend is observed for PI and Na-PI membranes; permeance enhancement as a function of temperature. Also, within the investigated pressure range, the transmembrane pressure has a limited effect on H_2 permeance. For all the measurement conditions, the H_2 permeance of GEN-PI membranes is lower than those of reported Na-PI membranes [19]. This is attributed to higher activation energies of GEN-PI than those reported for Na-PI tubular membranes [19]. Lower activation energies underline the lower energy barrier for gas diffusion. These results agree well with the obtained results for flat disc membranes in section 3.2. Unlike the results of flat membranes, which shows that lower permeance of PI membranes is related to the thicker selective layer, all GEN-PI and Na-PI membranes have a thickness in the range of 90–150 nm, slightly higher for GEN-PI membranes, 110–120 nm compared to 90–150 nm. In summary, while GEN-PI has a higher selectivity, the permeance is lower than Na-PI, showing the distinct performance of both types of polyPOSS-imide membranes on a larger scale regardless of the thickness of the selective layer.

Fig. 9 shows the mixed gas performance of GEN-PI at various temperatures (150, 200, and 250 °C) at a transmembrane pressure of 9 bar and its comparison with the literature data of Na-PI atop of tubular supports [19]. The selectivity of GEN-PI for all gas pairs decreases with increasing temperature in both pure and mixed gas, except for H_2/CO_2. This observation is in line with data obtained for flat disc membranes. Interestingly, in the case of pure gas selectivity of H_2/CO_2 and H_2/CH_4, a higher value is obtained for tubular membranes, 5.3 vs. 8 and 25.1 vs. 45.5, respectively, while the pure gas permeances are comparable for flat and tubular membranes (Fig. S4A). It could be related to the reduced mass transport resistance of the tubular membrane compared to the disc resulting from morphological differences and the higher operating pressure. Similar effects were observed in Ref. [19]. Unexpectedly, all pure gas selectivities of Na-PI membranes from literature, except for one membrane, GEN 7 [19], have a different trend than those of GEN-PI and increase as a function of temperature. It implies that all membranes, except for GEN 7, have defects and their influence on the gas selectivity becomes lower at higher temperature due to the drop in gas viscosity (assuming viscous flow through defects). These defects can be the result of salt formation, as shown by the XRD results, and its interference with the layer's formation during interfacial polymerization.

For all the gas pairs, the GEN-PI mixed gas selectivities are lower than pure gas selectivities. This is attributed to gas mixtures' effect on individual gas permeances, as shown in Fig. S3B. With increasing temperature, the permeance increases, agreeing well with the pure gas performance. The H_2 permeance is partially affected in mixed gas measurements and is reduced by 10% at 250 °C. This is probably due to the existence of a concentration polarization effect on the feed side as previously observed for high-flux Pd-based membranes [37]. When the H_2 permeance is so high, and the membrane is H_2 selective, a reduction in H_2 concentration and increment in the concentration of other gases occurs in the boundary layer [37,38]. While positive minor changes are observed in the permeance for CO_2 in mixed gas measurements, no remarkable changes are seen for CH_4. Moreover, an increase of 40% in the permeance of N_2 can be seen. A similar observation was also made for the Na-PI in the previous study [19]. The co-existence of CO_2 and CH_4 with other gases swells the polyPOSS imide layer and results in N_2 permeance enhancement [24]. All those changes in the gas permeance lead to the reduction in the mixture's gas pairs selectivity. It is noteworthy to mention that the long-term hydrothermal stability of polyPOSS-imide membranes was tested at 250 °C for 1000 h elsewhere [39], and the obtained results suggest that membrane's performance was preserved at unchanged condition.

In conclusion, membranes synthesized with SFPOSS show a pure gas selectivity of H_2/N_2 (34), H_2/N_2 (42), and H_2/CH_4 (8) at 200 °C, which is higher than those produced with HPPOSS. More importantly, out of three produced PI samples, none of them have any defects. On the contrary, Na-PI tubular membranes from the previous study [19] illustrate solid proof of deficiency on the selective layer for 5 membranes out of 6. Therefore, SFPOSS may have a better potential compared to HPPOSS to be used as a reactant in synthesizing polyPOSS-imide membranes on a large scale.

4. Conclusions

In this study, the effect of cations on the formation, imidization, and performance of polyPOSS-imide membranes atop lab-scaled flat disc and single-channel tubular supports for high temperature H_2 separation are investigated. Moreover, to upscale these membranes, a more straightforward fabrication procedure is assessed using SF-POSS cages rather than HP-POSS salt functionalized cages, which need deprotonation. For this purpose, three different lab-scale flat discs polyPOSS-imide membranes with HP-POSS and bases like LiOH, NaOH, and KOH, as a cation source, and one with SF-POSS, without cation, were prepared. Subsequently, to investigate the potential of SF-POSS, a tubular single-channel was fabricated. Finally, their performance was evaluated at different operating temperature and pressure.

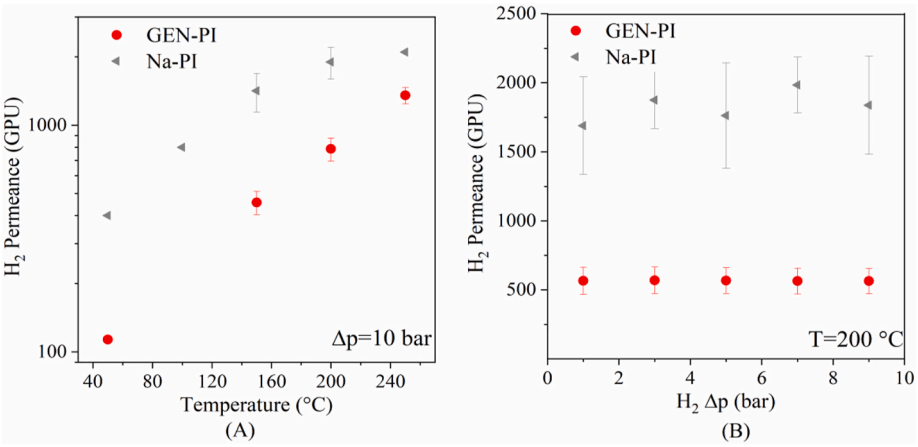

Fig. 8. Influence of temperature and pressure on GEN-PI membranes' performance compared with literature data [19] obtained for Na-PI membranes. (A) H_2 permeance as a function of temperature at Δp=10 bar, (B) H_2 permeance as a function of Δp at a temperature of 200 °C.

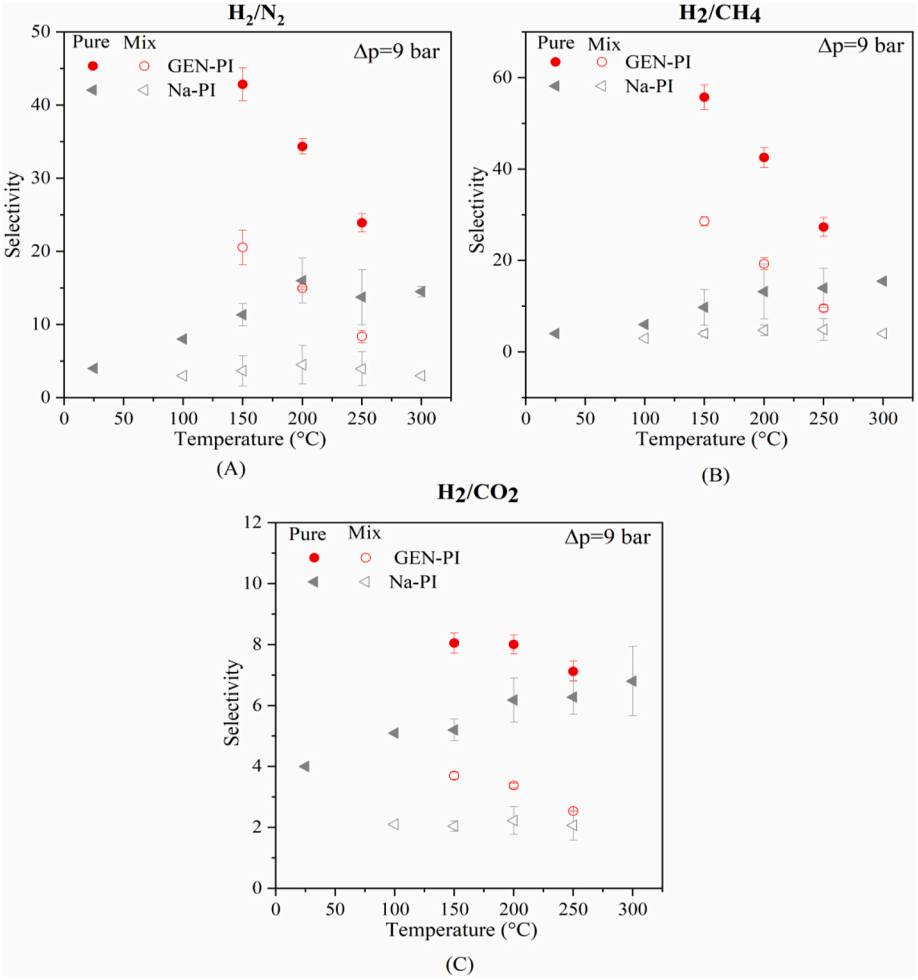

Fig. 9. PolyPOSS-imide separation performance using pure and quaternary gas mixtures at various temperatures and transmembrane pressure of 10 bar compared with literature data [19] obtained for Na-PI networks. (A) H_2/N_2 selectivity, (B) H_2/CH_4 selectivity, and (C) H_2/CO_2 selectivity as a function of temperature at Δp=9 bar. The calculated stage cut for transmembrane pressure of 10 bar is 53%.

It was found that all polyamic acid samples have the same cross-linking degree irrespective of the POSS source, and type of cations and, while each POSS cage is connected with 4 organic bridges. However, after imidization, an average number of imide groups per POSS cages reduces to 2 for PI networks, unlike M − PI, which retains the number of organic bridges. In the presence of cations, in the formed polyamic acid a carboxylic acid proton is replaced by an M^+ cation. This replacement prevents ring closure and reduces conversion yield during imidization. Different polyPOSS-imide layer thicknesses are obtained on top of flat disc supports, in the order Na-PI (69.4 nm) ≤ Li-PI (83.9 nm) < PI (100.3 nm) < K-PI(137.8 nm). This may be due to the distinct characteristics of the interface between the liquids in the presence of the salts, a diverse extent of the HP-POSS deprotonation originating from distinct strengths of the bases, and different electrostatic effects in the reaction zone. PI and K-PI membranes show higher ideal selectivity for H_2/N_2 and H_2/CH_4 with comparable H_2/CO_2 and have lower permeance and moderately lower permeability. These results advocate the scaling-up potential of polyPOSS-imide membranes using SF-POSS as a monomer (GEN-PI). The performance of GEN-PI membranes is in good agreement with the flat disc membranes. While the pure gas permeances are similar with the lab-scale membranes, a higher H_2/CO_2 and H_2/CH_4 are obtained, 5.3 versus 8, and 25.1 versus 45.5, respectively. This could be related to the lower mass transport resistance of tubular supports than the disc-shaped supports. Besides, GEN-PI performance is compared with previously studied Na-PI tubular membranes; in all measured conditions, GEN-PI membranes exhibit higher selectivity and lower permeance. More importantly, the average trend for GEN-PI H_2/N_2 and H_2/CH_4 is decreasing as a function of temperature. On the contrary, those selectivities increase with temperature for Na-PI membranes. This implies that the possibility of making defect free selective layers with SF-POSS as an initial monomer is much higher due to the absence of salt formation during interfacial polymerization. The findings signify that using SF-POSS in preparing large-scale defect free membranes can be beneficial. Also, the use of SF-POSS offers a more facile and straightforward procedure by omitting the deprotonation by the addition of a base.

Author statement

Farzaneh Radmanesh: Conceptualization, Data curation, Investigation, Methodology, Writing - original draft. **Monika Pilz:** Funding acquisition, Resources, Investigation, Writing - Review & Editing. **Luca Ansaloni**: Conceptualization, Investigation, Writing - Review & Editing. **Thijs A. Peters:** Funding acquisition, Data curation, Investigation, Writing - Review & Editing. **Eric Louradour:** Resources, Investigation, Writing - Review & Editing. **Henk van Veen:** Investigation, Writing - Review & Editing. **Dag Høvik:** Resources, Investigation, Writing - Review & Editing. **Mark Hempenius**: Data curation, Investigation, Writing - Review & Editing, Supervision. **Nieck E. Benes:** Funding acquisition, Conceptualization, Supervision, Writing - Review & Editing.

Declaration of competing interest

The authors declare that they have no known competing financial interests or personal relationships that could have appeared to influence the work reported in this paper.

Acknowledgment

This work is part of the GENESIS project and the authors acknowledge the financial support from the European Union's Horizon 2020 Research and Innovation Program under the Grant Agreement No. 760899. This publication reflects only the author's views and the European Union is not liable for any use that may be made of the information contained therein.

Appendix A. Supplementary data

Supplementary data to this article can be found online at https://doi.org/10.1016/j.memsci.2021.119524.

References

[1] A. Brunetti, F. Scura, G. Barbieri, E. Drioli, Membrane technologies for CO_2 separation, J. Membr. Sci. 359 (2010) 115–125, https://doi.org/10.1016/j.memsci.2009.11.040.

[2] H. Lin, B.D. Freeman, Materials selection guidelines for membranes that remove CO_2 from gas mixtures, J. Mol. Struct. 739 (2005) 57–74, https://doi.org/10.1016/j.molstruc.2004.07.045.

[3] B.B. Shrestha, K. Wakimoto, Z.G. Wang, A.P. Isfahani, T. Suma, E. Sivaniah, B. Ghalei, A facile synthesis of contorted spirobisindane-diamine and its microporous polyimides for gas separation, RSC Adv. 8 (2018) 6326–6330, https://doi.org/10.1039/C7RA12719G.

[4] L. Hu, S. Pal, H. Nguyen, V. Bui, H. Lin, Molecularly engineering polymeric membranes for H_2/CO_2 separation at 100–300° C, J. Polym. Sci. 58 (2020) 2467–2481, https://doi.org/10.1002/pol.20200220.

[5] S.S. Wu, J.C. Liang, Y.P. Shi, M.H. Huang, X.Y. Bi, Z.G. Wang, J. Jin, Design of interchain hydrogen bond in polyimide membrane for improved gas selectivity and membrane stability, J. Membr. Sci. 618 (2021), 118659, https://doi.org/10.1016/j.memsci.2020.118659.

[6] R.M. Laine, M.F. Roll, Polyhedral phenylsilsesquioxanes, Macromolecules 44 (2011) 1073–1109, https://doi.org/10.1021/ma102360t.

[7] M.J. Raaijmakers, M.A. Hempenius, P.M. Schön, G.J. Vancso, A. Nijmeijer, M. Wessling, N.E. Benes, Sieving of hot gases by hyper-cross-linked nanoscale-hybrid membranes, J. Am. Chem. Soc. 136 (2013) 330–335, https://doi.org/10.1021/ja410047u.

[8] Y. Yang, C.L. Muhich, M.D. Green, Kinetics and mechanisms of polycondensation reactions between aryl halides and bisphenol A, Polym. Chem. 11 (2020) 5078–5087, https://doi.org/10.1039/D0PY00740D.

[9] Y. Mansourpanah, S.S. Madaeni, A. Rahimpour, Fabrication and development of interfacial polymerized thin-film composite nanofiltration membrane using different surfactants in organic phase; study of morphology and performance, J. Membr. Sci. 343 (2009) 219–228, https://doi.org/10.1016/j.memsci.2009.07.033.

[10] X.C. Fan, Y.L. Su, X.T. Zhao, Y.F. Li, R.N. Zhang, J.J. Zhao, Z.Y. Jiang, J.N. Zhu, Y. Y. Ma, Y. Liu, Fabrication of polyvinyl chloride ultrafiltration membranes with stable antifouling property by exploring the pore formation and surface modification capabilities of polyvinyl formal, J. Membr. Sci. 464 (2014) 100–109, https://doi.org/10.1016/j.memsci.2014.04.005.

[11] J. Lee, R. Wang, T.H. Bae, A comprehensive understanding of co-solvent effects on interfacial polymerization: interaction with trimesoyl chloride, J. Membr. Sci. 583 (2019) 70–80, https://doi.org/10.1016/j.memsci.2019.04.038.

[12] H.G. Linde, R.T. Gleason, Cation interactions with polyamic acids, J. Polym. Sci. B Polym. Phys. 27 (1989) 1485–1497, https://doi.org/10.1002/polb.1989.090270710.

[13] S. Ikeda, K. Akamatsu, H. Nawafune, T. Nishino, S. Deki, Formation and growth of copper nanoparticles from ion-doped precursor polyimide layers, J. Phys. Chem. B 108 (2004) 15599–15607, https://doi.org/10.1021/jp0478559.

[14] L.F. Villalobos, R. Hilke, F.H. Akhtar, K.V. Peinemann, Fabrication of polybenzimidazole/palladium nanoparticles hollow fiber membranes for hydrogen purification, Adv. Energy Mater. 8 (2018), 1701567, https://doi.org/10.1002/aenm.201701567.

[15] S. Serchenkova, M. Shablygin, T. Kravchenko, Z. Oprits, G. Kudryavtsev, Study of the cyclodehydration reaction of benzamido acid systems, Polym. Sci. USSR 20 (1978) 1284–1294, https://doi.org/10.1016/0032-3950(78)90269-1.

[16] M. Dalwani, J. Zheng, M. Hempenius, M.J. Raaijmakers, C.M. Doherty, A.J. Hill, M. Wessling, N.E. Benes, Ultra-thin hybrid polyhedral silsesquioxane–polyamide films with potentially unlimited 2D dimensions, J. Mater. Chem. 22 (2012) 14835–14838, https://doi.org/10.1039/C2JM31941A.

[17] P. Karakiliç, C. Huiskes, M.W. Luiten-Olieman, A. Nijmeijer, L. Winnubst, Sol-gel processed magnesium-doped silica membranes with improved H_2/CO_2 separation, J. Membr. Sci. 543 (2017) 195–201, https://doi.org/10.1016/j.memsci.2017.08.055.

[18] M.J.T. Raaijmakers, M. Wessling, A. Nijmeijer, N.E. Benes, Hybrid polyhedral oligomeric silsesquioxanes-imides with tailored intercage spacing for sieving of hot gases, Chem. Mater. 26 (2014) 3660–3664, https://doi.org/10.1021/cm500691e.

[19] L. Ansaloni, E. Louradour, F. Radmanesh, H. van Veen, M. Pilz, C. Simon, N. E. Benes, T.A. Peters, Upscaling polyPOSS-imide membranes for high temperature H_2 upgrading, J. Membr. Sci. 620 (2021), 118875, https://doi.org/10.1016/j.memsci.2020.118875.

[20] H. Fukuzumi, S. Fujisawa, T. Saito, A. Isogai, Selective permeation of hydrogen gas using cellulose nanofibril film, Biomacromolecules 14 (2013) 1705–1709, https://doi.org/10.1021/bm400377e.

[21] M. Shimizu, T. Saito, A. Isogai, Water-resistant and high oxygen-barrier nanocellulose films with interfibrillar cross-linkages formed through multivalent metal ions, J. Membr. Sci. 500 (2016) 1–7, https://doi.org/10.1016/j.memsci.2015.11.002.

[22] J.I. Goldstein, D.E. Newbury, J.R. Michael, N.W. Ritchie, J.H.J. Scott, D.C. Joy, Scanning Electron Microscopy and X-Ray Microanalysis, Springer, 2017.

[23] A. Sthoer, J. Hladílková, M. Lund, E. Tyrode, Molecular insight into carboxylic acid–alkali metal cations interactions: reversed affinities and ion-pair formation revealed by non-linear optics and simulations, Phys. Chem. Chem. Phys. 21 (2019) 11329–11344, https://doi.org/10.1016/10.1039/C9CP00398C.

[24] M.J.T. Raaijmakers, W. Ogieglo, M. Wiese, M. Wessling, A. Nijmeijer, N.E. Benes, Sorption behavior of compressed CO_2 and CH_4 on ultrathin hybrid poly(POSS-imide) layers, ACS Appl. Mater. Interfaces 7 (2015) 26977–26988, https://doi.org/10.1021/acsami.5b08286.

[25] M.J.T. Raaijmakers, E.J. Kappert, A. Nijmeijer, N.E. Benes, Thermal imidization kinetics of ultrathin films of hybrid poly(POSS-imide)s, Macromolecules 48 (2015) 3031–3039, https://doi.org/10.1021/acs.macromol.5b00473.

[26] B. Thomson, Y. Park, P.C. Painter, R.W. Snyder, Hydrogen-bonding in poly(amic Acid)s, Macromolecules 22 (1989) 4159–4166, https://doi.org/10.1021/ma00201a005.

[27] Q. Li, Z.P. Liao, X.F. Fang, J. Xie, L.H. Ni, D.P. Wang, J.W. Qi, X.Y. Sun, L.J. Wang, J.S. Li, Tannic acid assisted interfacial polymerization based loose thin-film composite NF membrane for dye/salt separation, Desalination 479 (2020), 114343, https://doi.org/10.1016/j.desal.2020.114343.

[28] W.M. Nielen, J.D. Willott, Z.M. Esguerra, W.M. de Vos, Ion specific effects on aqueous phase separation of responsive copolymers for sustainable membranes, J. Colloid Interface Sci. 576 (2020) 186–194, https://doi.org/10.1016/j.jcis.2020.04.125.

[29] M. Omidvar, C.M. Stafford, H. Lin, Thermally stable cross-linked P84 with superior membrane H_2/CO_2 separation properties at 100° C, J. Membr. Sci. 575 (2019) 118–125, https://doi.org/10.1016/j.memsci.2019.01.003.

[30] K.A. Stevens, J.D. Moon, H. Borjigin, R. Liu, R.M. Joseph, J.S. Riffle, B.D. Freeman, Influence of temperature on gas transport properties of tetraaminodiphenylsulfone (TADPS) based polybenzimidazoles, J. Membr. Sci. 593 (2020), 117427, https://doi.org/10.1016/j.memsci.2019.117427.

[31] X. Li, R.P. Singh, K.W. Dudeck, K.A. Berchtold, B.C. Benicewicz, Influence of polybenzimidazole main chain structure on H_2/CO_2 separation at elevated temperatures, J. Membr. Sci. 461 (2014) 59–68.

[32] D. Brown, S. Neyertz, M.J.T. Raaijmakers, N.E. Benes, Sorption and permeation of gases in hyper-cross-linked hybrid poly(POSS-imide) networks: an in silico study, J. Membr. Sci. 577 (2019) 113–128, https://doi.org/10.1016/j.memsci.2014.03.008.

[33] M. Kanezashi, Y. Tomarino, H. Nagasawa, T. Tsuru, Tailoring the molecular sieving properties and thermal stability of carbonized membranes containing polyhedral oligomeric silsesquioxane (POSS)-polyimide via the introduction of norbornene, J. Membr. Sci. 582 (2019) 59–69, https://doi.org/10.1016/j.memsci.2019.04.003.

[34] L. Yu, M. Kanezashi, H. Nagasawa, T. Tsuru, Role of amine type in CO_2 separation performance within amine functionalized silica/organosilica membranes: a Review, Appl. Sci. 8 (2018) 1032, https://doi.org/10.3390/app8071032.

[35] Y. Zhang, W.H. Lee, J.G. Seong, J.Y. Bae, Y. Zhuang, S. Feng, Y. Wan, Y.M. Lee, Alicyclic segments upgrade hydrogen separation performance of intrinsically microporous polyimide membranes, J. Membr. Sci. 611 (2020), 118363, https://doi.org/10.1016/j.memsci.2020.118363.

[36] M. Shan, X. Liu, X. Wang, Z. Liu, H. Iziyi, S. Ganapathy, J. Gascon, F. Kapteijn, Novel high performance poly(p -phenylene benzobisimidazole) (PBDI) membranes fabricated by interfacial polymerization for H_2 separation, J. Mater. Chem. A. 7 (2019) 8929–8937, https://doi.org/10.1039/C9TA01524H.

[37] T.A. Peters, M. Stange, H. Klette, R. Bredesen, High pressure performance of thin Pd–23%Ag/stainless steel composite membranes in water gas shift gas mixtures; influence of dilution, mass transfer and surface effects on the hydrogen flux, J. Membr. Sci. 316 (2008) 119–127, https://doi.org/10.1016/j.memsci.2007.08.056.

[38] Y.W. Budhi, W. Suganda, H.K. Irawan, E. Restiawaty, M. Miyamoto, S. Uemiya, N. Nishiyama, M. van Sint Annaland, Hydrogen separation from mixed gas (H_2, N_2) using Pd/Al_2O_3 membrane under forced unsteady state operations, Int. J. Hydrogen Energy 45 (2020) 9821–9835, https://doi.org/10.1016/j.ijhydene.2020.01.235.

[39] L. Ansaloni, M. Sarić, E. Louradour, F. Radmanesh, J.W. Dijkstra, M. Pilz, D. Høvik, N. Benes, Y. van Delft, T.A. Peters, Stability investigation of polyPOSS-imide membranes for H2 purification and their application in the steel industry. 15th Greenhouse Gas Control Technologies Conference 15-18 March 2021, 2021. https://ssrn.com/abstract=3811364.